Electronic Supplementary Material (ESI) for Journal of Materials Chemistry A.

Origin of extra capacity in nitrogen-doped porous carbon nanofibers for high-performance potassium ion batteries

Fang Liu [a, b], Jiashen Meng [a], Fanjie Xia [a, b], Ziang Liu [a], Haoyang Peng [a, b], Congli Sun [a, b], Linhan Xu* [d, e], Gustaaf Van Tendeloo [b, c], Liqiang Mai* [a], Jinsong Wu * [a, b]

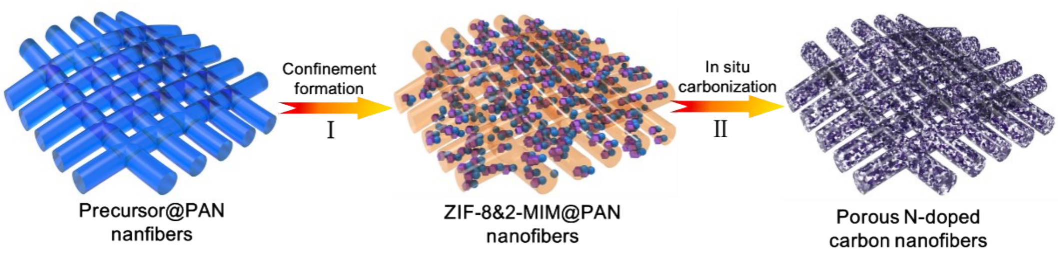

Figure S1. Schematic illustration of the formation process of freestanding porous NCNF.

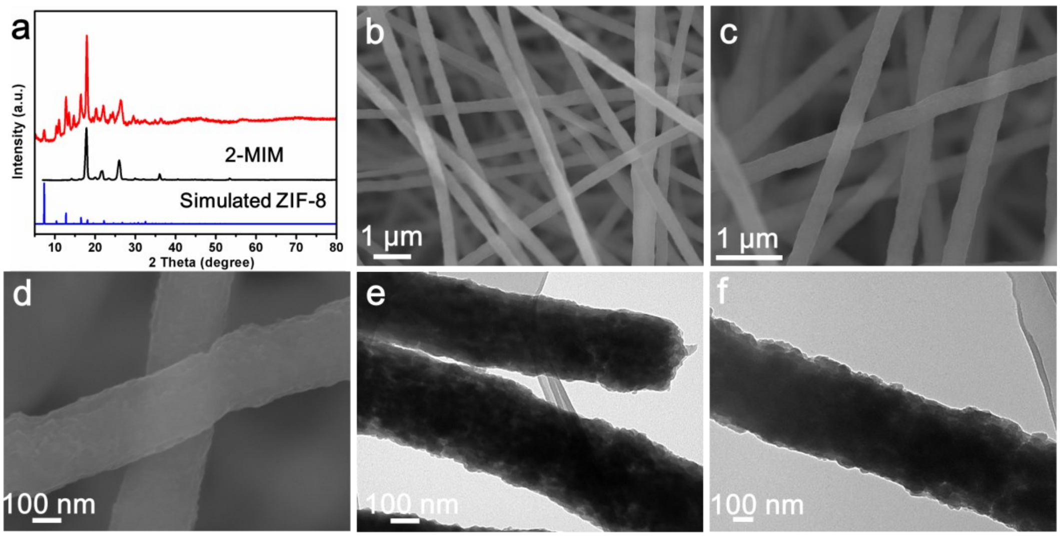

Figure S2. (a) XRD patterns of ZIF-8&2-MIM@PAN nanofibers. (b-d) SEM images of ZIF-8&2-MIM@PAN nanofibers. (e, f) TEM images of ZIF-8&2-MIM@PAN nanofibers.

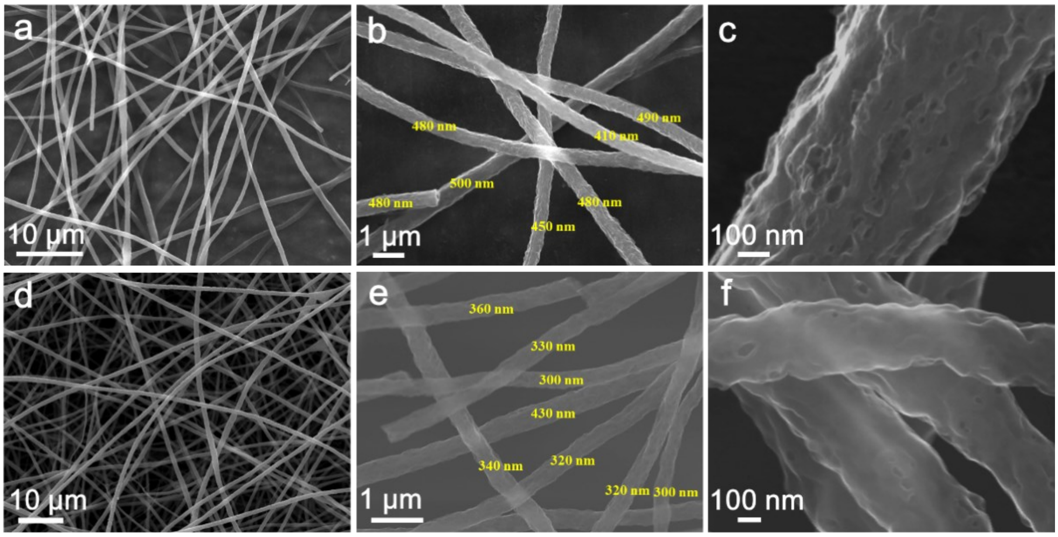

Figure S3. (a-c) SEM images of the NCNF-800 sample. (d-f) SEM images of NCNF-1000.

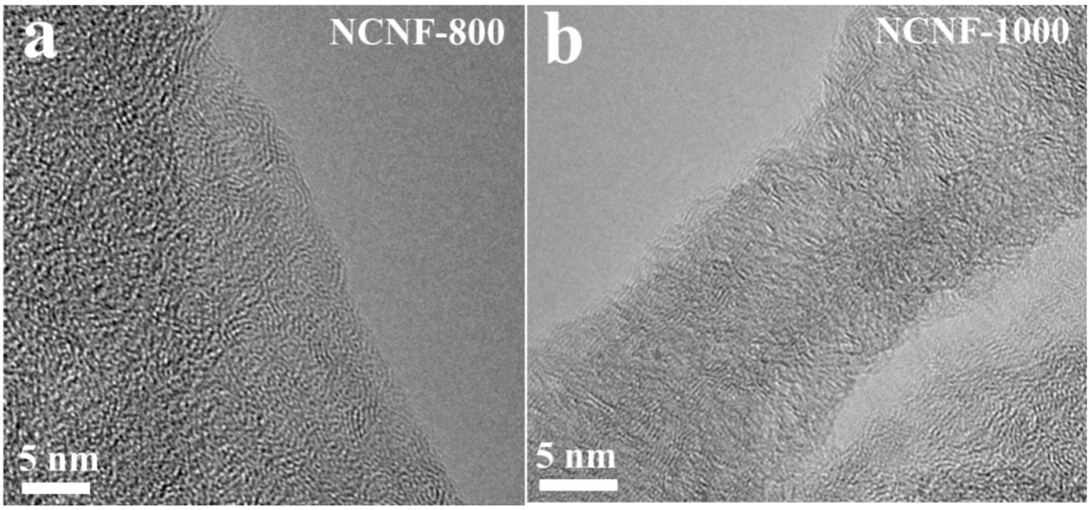

Figure S4. (a) HRTEM images of the NCNF-800 sample. (b) HRTEM images of NCNF-1000 sample.

Table S1. A summary of Raman results for NCNF-800 and NCNF-1000 samples.

Temperature (°C)	I_D	I_G	I_D/I_G	Average size of crystalline domains (nm)
800	1241360	463109	2.68	14.35696
1000	378872	157420	2.41	15.98985

Tuinstra-Koenig Relation：

$$L_a = \left(2.4 \times 10^{-10}\right) \times \lambda^4 \times \left(I_D / I_G\right)^{-1}$$

L_a is the average size of the in-plane sp^2-domains; λ is the laser excitation wavelength (633 nm); I_D is the intensity of the D-peak; I_G is the intensity of the G-peak. The smaller the intensity of the D-peak, the larger *La* and the larger average size of the crystalline domains.

Table S2. A summary of the relative contents of C, N and H in NCNF-800 and NCNF-1000 samples.

Samples	C (wt%)	N (wt%)	H (wt%)
NCNF-800	**91.6**	**6.9**	**1.6**
NCNF-1000	**97.4**	**1.9**	**0.7**

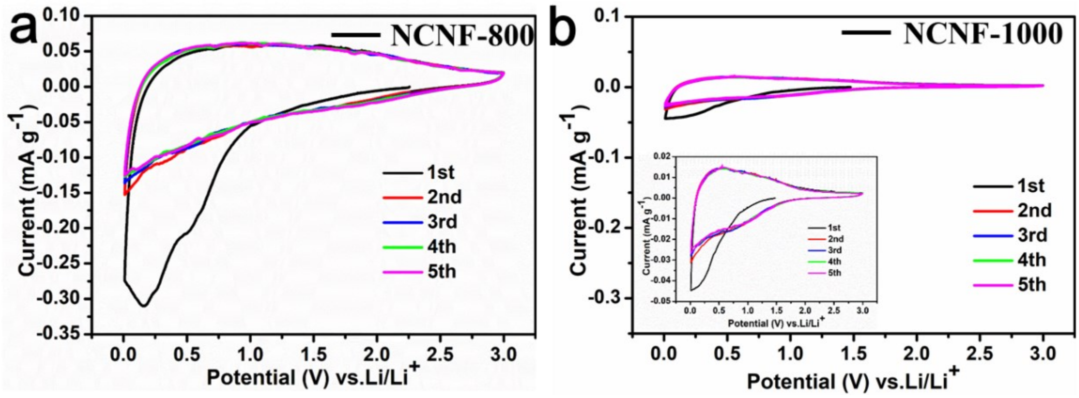

Figure S5. (a) First four CV curves of the NCNF-800 sample tested at a scan rate of 0.2 mV·s^{-1} in a potential range from 0.01 to 3.0 V versus K^+/K. (b) First four CV curves of the NCNF-1000 sample tested at a scan rate of 0.2 mV·s^{-1} in a potential range from 0.01 to 3.0 V versus K^+/K. Inset of (b) is magnified CV curves.

Table S3 A comparison of discharge capacities and the position of the π*-peak and σ*-peak for different discharge voltages at 100 mA g^{-1} current density between NCNF-800 and NCNF-1000.

	Discharge voltage (V)	**OCV**	**2**	**1.5**	**1**	**0.5**	**0.01**
NCNF-800	**The discharge capacity (mAh g^{-1})**	0	5	30	72	153	280
	The position of π*-peak (eV)	285.3	-	-	285.3	285.3	287.4
	The position of σ*-peak (eV)	291.8	-	-	292.0	292.1	291.4
NCNF-1000	**The discharge capacity (mAh g^{-1})**		0	3	28	70	180
	The position of π*-peak (eV)	284.8	-	-	285.1	285.6	286
	The position of σ*-peak (eV)	291.8	-	-	291.8	291.8	292.6

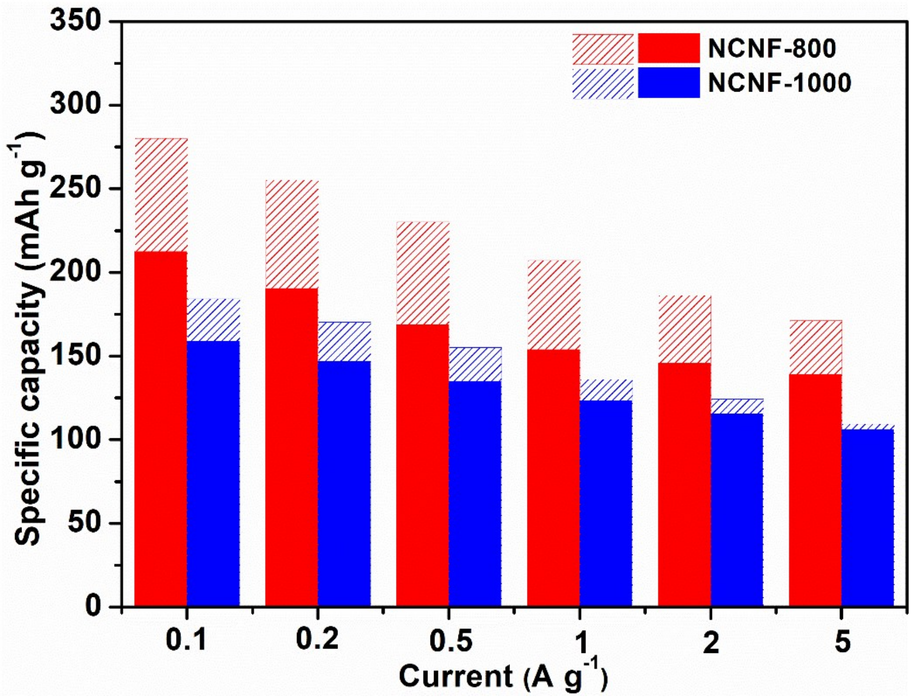

Figure S6. Capacity distribution from the high-voltage region (shaded) and from the low-voltage region (solid) for both NCNF-800 and the NCNF-1000 electrodes at different current densities.

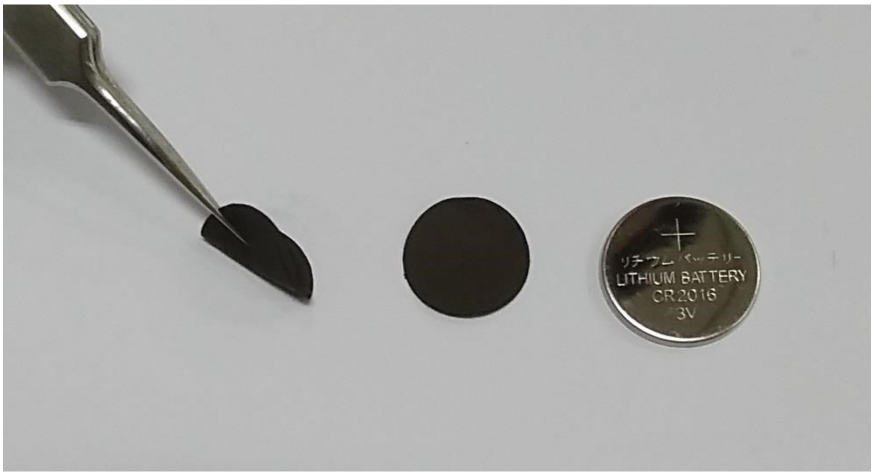

Figure S7. The optical image of a freestanding anode based on the NCNT sample.

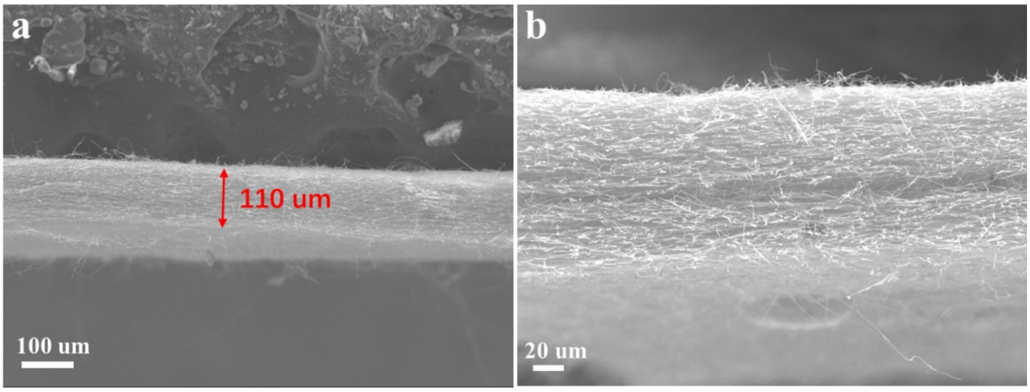

Figure S8. The cross-section SEM images of NCNF-800

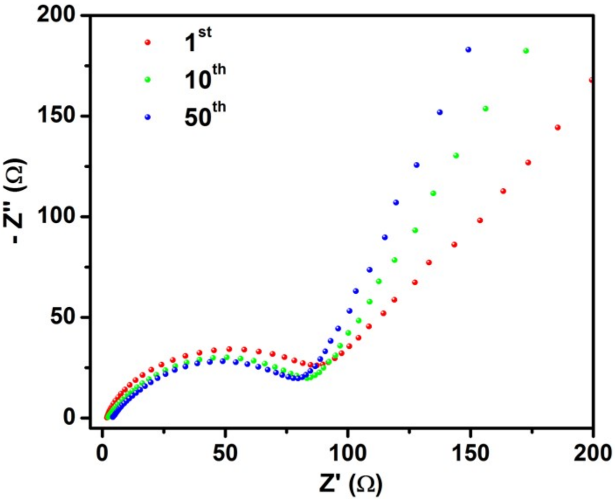

Figure S9. The Nyquist plots of NCNF-800 at different cycles.

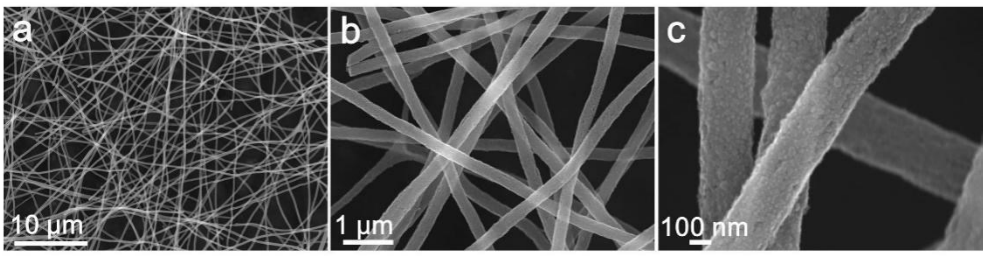

Figure S10. (a-c) SEM images of NCNF-800 after 1000 cycles at a current density of 2000 mA·g^{-1}.

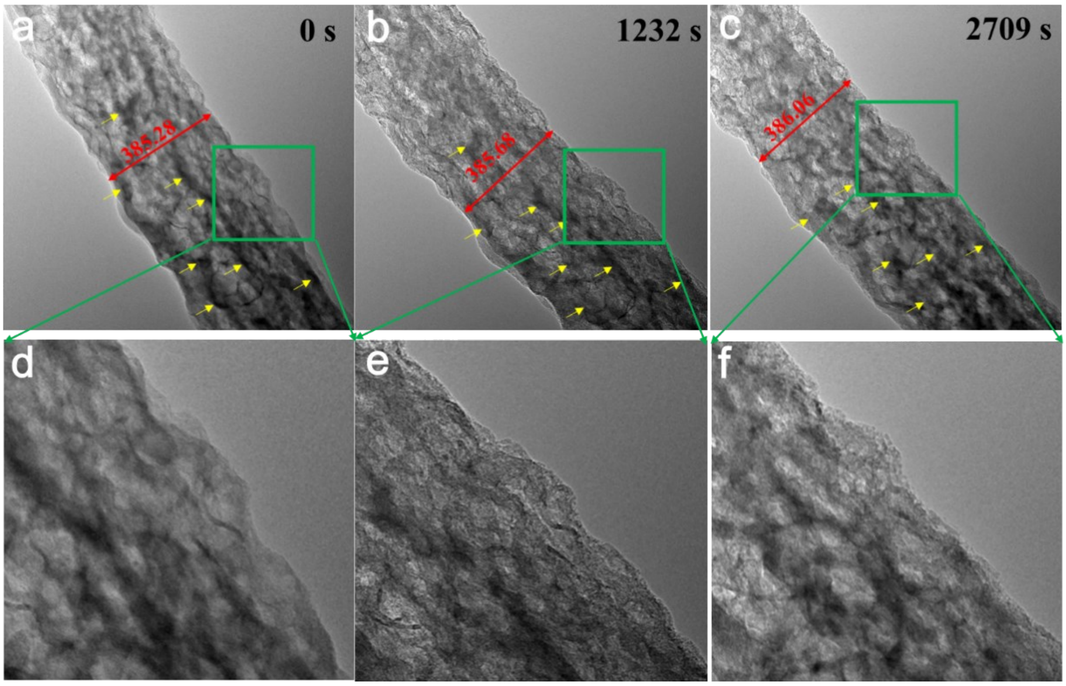

Figure S11. (a-c) The morphological evolution of NCNF-800 during the potassiation reaction. (d-e) First four CV curves of NCNF-1000 sample tested at a scan rate of 0.2 mV·s^{-1} in the potential range from 0.01 to 3.0 V versus K^+/K.

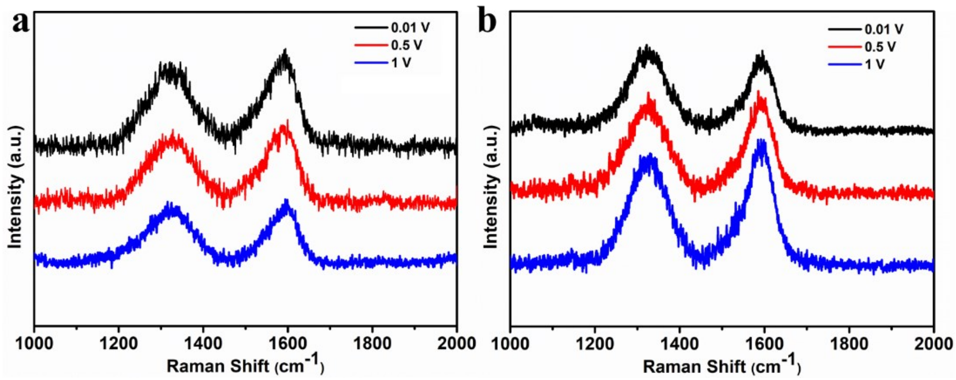

Figure S12. Raman spectra of (a) NCNF-800 and (b) NCNF-1000 at different potentials during the discharge process.

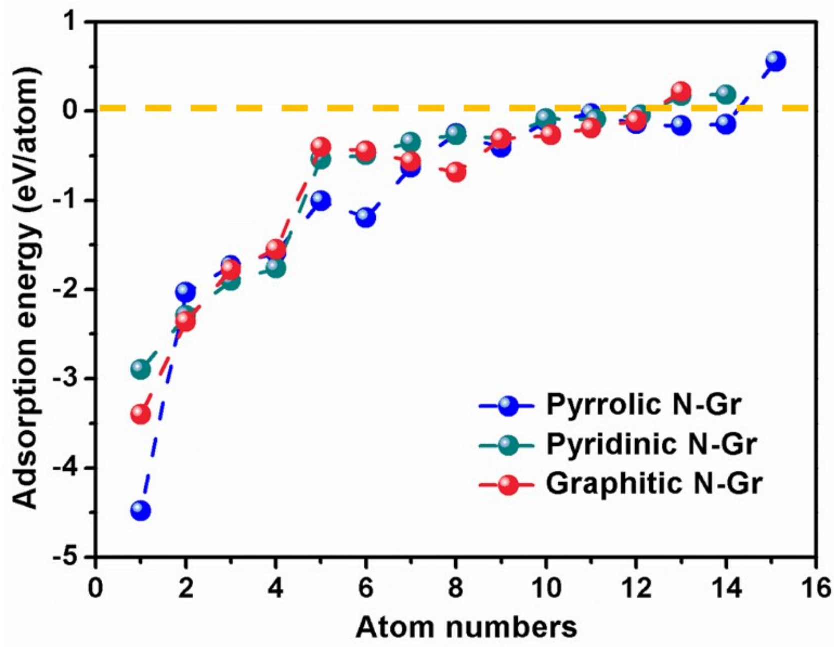

Figure S13. The variation of the average adsorption energy along with the number of K atoms for different N-doped graphene.